[redacted]

50
3/11
Fast Reactor
& Data Journal
No stock
NR

[redacted]

Westinghouse Advanced Reactors Division

P4581

DISCLAIMER

WARD 4135-3

FAST REACTOR FUEL PERFORMANCE MODEL DEVELOPMENT

A. Boltax, P. Murray, and A. Biancheria

Approved by P. Murray
P. Murray
Project Manager

Contract AT(30-1)-4135
U. S. Atomic Energy Commission

Submitted to AEC-NYOO in February 1970

Westinghouse Electric Corporation
Advanced Reactors Division
P. O. Box 158
Madison, Pennsylvania 15663

LEGAL NOTICE

This report was prepared as an account of Government sponsored work. Neither the United States, nor the Commission, nor any person acting on behalf of the Commission:

A. Makes any warranty or representation, expressed or implied, with respect to the accuracy, completeness, or usefulness of the information contained in this report, or that the use of any information, apparatus, method, or process disclosed in this report may not infringe privately owned rights; or

B. Assumes any liabilities with respect to the use of, or for damages resulting from the use of any information, apparatus, method, or process disclosed in this report.

As used in the above, "person acting on behalf of the Commission" includes any employe or contractor of the Commission, or employe of such contractor, to the extent that such employe or contractor of the Commission, or employe of such contractor prepares, disseminates, or provides access to, any information pursuant to his employment or contract with the Commission, or his employment with such contractor.

Printed in the United States of America
Available from
Clearinghouse for Federal Scientific and Technical Information
National Bureau of Standards, U. S. Department of Commerce
Springfield, Virginia 22151
Price: Printed Copy $3.00; Microfiche $0.65

ABSTRACT

This report is a review of the status of fast reactor fuel performance model development, involving the OLYMPUS and CYGRO-F codes. Input information in several critical areas is examined including the swelling, irradiation creep, and ductility of stainless steel cladding; and the swelling and plasticity of mixed oxide fuel. The predictions from the two codes are illustrated by parametric studies and application to high fluence/burnup ratio fuel rods of interest to the Liquid Metal Fast Breeder Reactor (LMFBR) Program.

TABLE OF CONTENTS

LIST OF FIGURES

LIST OF TABLES

INTRODUCTION

GENERAL

The AEC Liquid Metal Fast Breeder Reactor (LMFBR) Program is supporting the development of stainless steel clad mixed oxide fuel performance models to predict fuel rod behavior, including cladding dimensional changes (distinguishing between stainless steel swelling and creep strain), principal cladding stresses, cladding failure limits, fission gas release, fuel temperature distribution, fuel restructuring, etc. as a function of fuel pin design parameters. These parameters include:

1. Fuel form (solid and annular pellets, powder)
2. Fuel density (amount and distribution of porosity)
3. Initial fuel-clad gap
4. Cladding thickness and type (cold-worked and solution treated)
5. Operating parameters (linear power rating, cladding temperature burnup, fluence, and fluence/burnup ratio)
6. Design overpower and transient conditions

At the present time, there is no single model or collection of models which meets all of the design requirements for the fast reactor fuel performance prediction. This paper describes the WARD program that is directed toward providing an evolutionary development of fast reactor fuel performance models. The characteristics of this evolutionary program include:

1. Continuous updating of the models with generation of new data and theoretical understanding
2. Use of the models to define the need for critical experimental data
3. Application of the models for design purposes with appropriate confidence limits to assure conservative design

TECHNICAL APPROACH

The selected technical approach for the development of fuel performance models involves the parallel development of a phenomenological model which meets the immediate conceptual design needs of the LMFBR program, and a longer range model development program which provides a complete formulation of fuel behavior. The first approach has given rise to a series of codes called OLYMPUS[1] which have been utilized in conceptual design studies.

The second approach, based on the CYGRO-2 Code[2], currently involves a sensitivity analysis study. This Code will be available for design use in the spring of 1970.

The principle steps involved in fuel performance code development are well known [2-4] and include: data analysis, model development, sensitivity analysis, comparisons with test data, and design application.

DATA ANALYSIS

It is axiomatic that the design usefulness of a fuel behavior model is in direct proportion to the availability of reliable and relevant experimental data. Table 1 shows a comparison of the conceptual fuel performance parameters for the Fast Flux Test Facility (FFTF) with the range of available data obtained from test reactor (EBR-II and DFR) irradiation experiments on stainless steel clad mixed oxide fuel pins. Examination of Table 1 reveals two major limitations in the experimental data relative to the FFTF design parameters. Current fast reactor irradiation experience is limited to about one-half of the fast flux, fluence, or fluence/burnup ratio expected in FFTF. Also, data are not available at the combination of fuel operating parameters (particularly power level, burnup, and cladding temperature) at the inlet and outlet ends of the FFTF reactor. It is clear that extrapolation to twice the fluence and also extrapolation to critical combinations of power level, burnup, and cladding temperature will be required. Thus, all fuel pin properties and phenomena affected by flux, fluence, fluence/ burnup ratio, power level, burnup, and cladding temperature must be considered in the required extrapolation. The main properties and phenomena affected by this extrapolation are the swelling, irradiation creep, ductility of the cladding, and the swelling and plasticity of the fuel. The current state of knowledge of these properties and phenomena will be briefly reviewed to define some of the basic inputs to the OLYMPUS and CYGRO codes.

STAINLESS STEEL SWELLING

Battelle-Northwest Laboratory (BNWL) and WARD are providing a continuing review of stainless steel swelling data in support of FFTF core design studies. The swelling equations recommended in August, 1969[5] are as follows:

Solution-treated 304 or 316 SS

$$\% \frac{\Delta V}{V} = 4.3 \times 10^{-49} (\phi t)^{1.71} \exp\left(\frac{3.57 \times 10^4}{T} - \frac{1.38 \times 10^7}{T^2} \right) \qquad (1)$$

20% Cold-Worked 316 SS

$$\% \frac{\Delta V}{V} = 10^{-36} (\phi t)^{1.69} \{ \exp(-7800/RT) - 5.48 \times 10^3 \exp(-25300/RT) \} \qquad (2)$$

Table 1. Comparison of FFTF Fuel Performance Parameters and Irradiation Experience on Mixed Oxide Fuel Pins

Region	Cladding Temperature Range (°C)	Power Level (kw/ft)	%BU	Fast Flux (E>0.1 Mev) (10^{15})	Fast Fluence (E>0.1 Mev) (10^{22})	Fluence/BU Ratio (10^{22}/% BU)
FFTF FUEL PERFORMANCE PARAMETERS[a]						
Inlet	350-380	5-8	4-6	1.6-2.9	4.5-7.8	1.1-1.3
Core	430-520	12.4	8.6	4.3	12.0	1.4
Outlet	500-620	5-8	4-6	1.6-2.9	4.5-7.8	1.1-1.3
IRRADIATION EXPERIENCE						
Inlet	350-380	9-15	3-7	1-2	2-6	0.5-0.9
Core	430-520	8-15	3-7	1-2	2-6	0.5-0.9
Outlet	500-620	7-15	3-7	1-2	2-6	0.5-0.9

[a]Representative of LMFBR

where

$\% \frac{\Delta V}{V}$ is the volume percent stainless steel swelling

ϕt the fast fluence (E > 0.1 Mev)

T the absolute temperature, °K

R the gas constant, calories/mole °K

Figures 1 and 2 illustrate the swelling relationships at three levels of fluence.[b] A statistical analysis of the data utilized in obtaining Equations (1) and (2) shows that the 95% confidence on the mean is typically ± 30% at a fluence of 5 x 10^{22} (E > 0.1 Mev), and $^{+100}_{-50}$ % at 2 x 10^{23} n/cm^2 (E > 0.1 Mev). For fuel pin design studies, where one is concerned with the behavior of individual fuel rods, the 95% confidence boundaries of the prediction interval for the next observation are used. The range of values for 95% confidence on the prediction interval is typically $^{+100}_{-50}$ % of the mean value up to a fluence of 6 x 10^{22} (E > 0.1 Mev). Since stainless steel swelling provides free volume within the pin for fuel swelling, the lower boundary of swelling values will be critical in determining burnup limits or maximum allowable fuel smear density. On the other hand, use of the values given by the upper swelling boundary may give rise to problems involving the fuel/cladding gap and/or differential stainless steel swelling.

In the OLYMPUS and CYGRO illustrations given later in this report, 20% cold worked 316 SS is the only cladding material considered. The concentration of effort on cold worked 316 SS is due to its lower swelling rate and the major effect fuel rod swelling has on fuel subassembly design.

IRRADIATION CREEP OF STAINLESS STEELS

The current position on irradiation creep of stainless steels is highly uncertain due to the lack of pertinent data. Therefore, irradiation creep is not included in the present OLYMPUS and CYGRO codes. However, a general position on irradiation creep in structural and cladding materials is developing, and forms a framework for future analysis work on stainless steels. Based on a review of the literature, principally the work of Lewthwaite, et.al[6], Hesketh[7], and Nichols[8], the following generalized equations can be used to describe in-reactor creep strain, ε_{Total}.

$$\varepsilon_{Total} = \varepsilon_{Thermal} + \dot{\varepsilon}_{Irradiation} \quad (3)$$

$$\varepsilon_{Irradiation} = A\,\sigma\,(1 - e^{-\phi t/B}) + C\,\sigma^{x}\,\phi\,t \quad (4)$$

---

[b] Figures 1 and 2 present extrapolations of Equations (1) and (2) to fluences of 2 x 10^{23} (E > 0.1 Mev) with no regard for possible swelling saturation mechanisms.

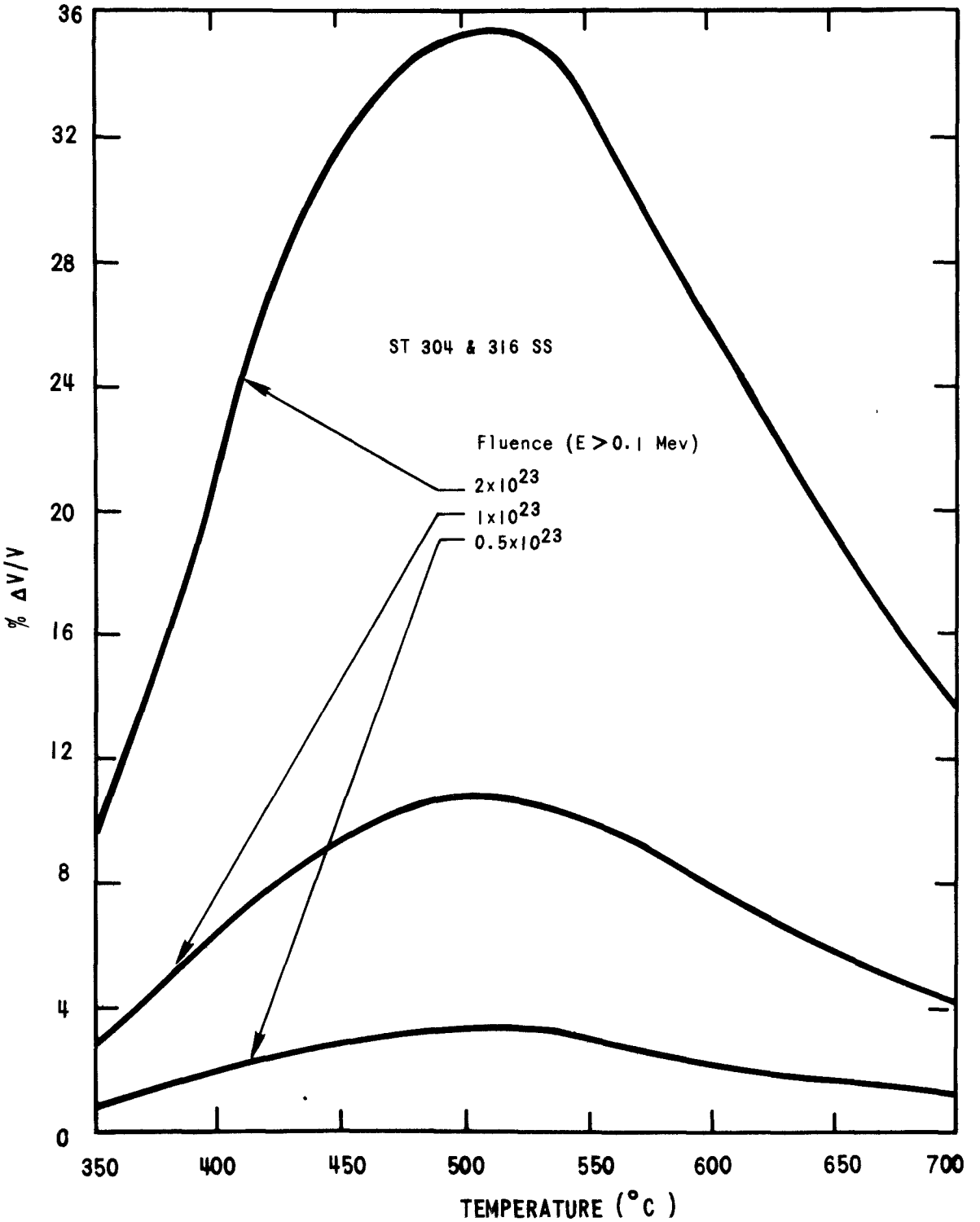

Figure 1. Swelling of Solution Treated 304 and 316 Stainless Steel as a Function of Temperature and Fluence.

3469-1

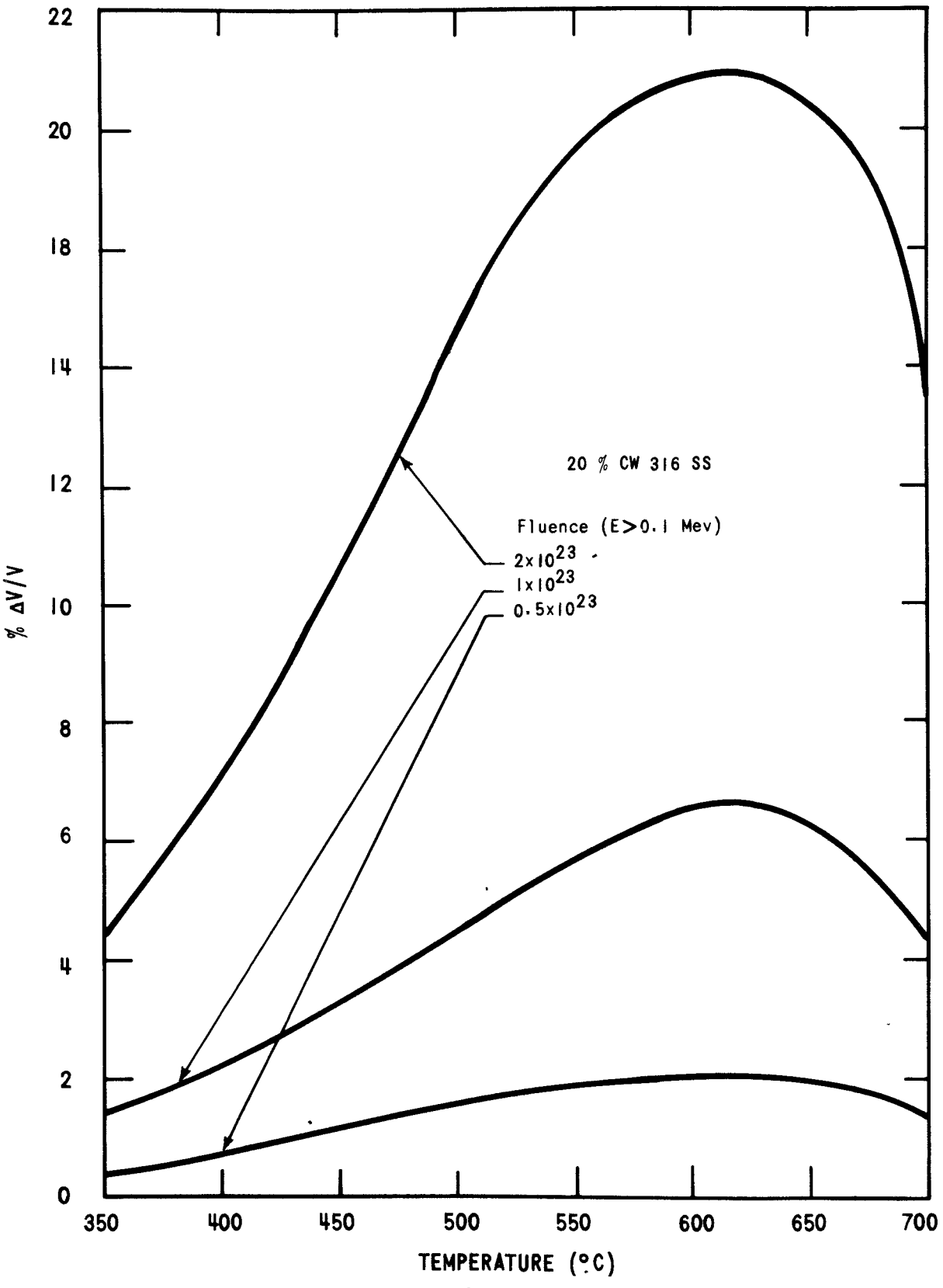

Figure 2. Swelling of 20% Cold Worked 316 Stainless Steel as a Function of Temperature and Fluence.

3469-2

where

σ is the creep stress

ϕ is the fast flux (E > 0.1 Mev)

t is the irradiation time

A, B, C are constants (dependent on temperature)

x is an exponent (equal to unity when $\sigma <$ 15,000 psi)

The first term in Equation (4) defines a transient irradiation induced creep strain which, for 316 stainless steel, saturates at relatively low fluence ($\sim 10^{21}$ n/cm^2)[6] From the work of Hesketh,[7] the A and C terms vary inversely with temperature, whereas B varies directly with temperature. The available data also indicate that x is unity for low levels of stress. For stainless steels, irradiation creep is expected to be most significant below 500°C. The irradiation creep model given by Equations (3) and (4) will be incorporated in future versions of the OLYMPUS and CYGRO-F codes.

In a recent paper, Nichols[8] noted that irradiation creep in Zircaloy, which is quite similar in nature to that in stainless steels (i.e. transient and steady state irradiation creep with similar temperature dependency and greater creep for cold-worked material[7]), gives rise to deformation behavior similar to that in superplastic materials. Nichols concludes that there is no ductility limit associated with the type of irradiation creep indicated by Equation (4). This conclusion indicates that irradiation creep provides a strain mechanism which will not give rise to local cladding necking and associated failure. However, since total creep strain is the sum of irradiation and thermal creep, and thermal creep can cause necking and failure, a thermal creep ductility limit must be considered.

CLADDING DUCTILITY

Large uncertainty exists on the allowable levels and the various mechanisms of cladding strain. The sources of cladding strain considered include thermal strain, elastic strain, primary and secondary thermal creep strain, and irradiation induced transient and steady state creep strain. There is also some concern regarding the growth of voids under stress at high cladding temperatures (600-700°C). Experimental fuel pin irradiation experiments in EBR-II and DFR indicate satisfactory fuel pin performance with solution-treated cladding to 1.5% creep strain [9,10], and 0.8% creep strain with 20% cold-worked cladding.[10,11] Current FFTF design studies are based on a conservative 0.2% limit for all sources of mechanical strain. An illustration of the application of this design limit to fuel pin design appears later in the discussion of results obtained using the OLYMPUS code.

FUEL SWELLING AND PLASTICITY

Another area of significant uncertainty involves the definition of fuel swelling as a function of temperature, burnup, burnup rate, and degree of restraint. The current versions of OLYMPUS utilize an empirically determined fuel swelling value of 1.3% $\Delta V/V$ per atom % burnup (BU) for fuel operating between 8-15 kw/ft.[c] Present analysis utilizing CYGRO indicates that fuel swelling can be treated as a function of fuel power level. Empirical estimates of fuel swelling relationships are discussed along with the CYGRO code.

The OLYMPUS and CYGRO codes treat fuel plasticity by different but related techniques. In the OLYMPUS code, fuel plasticity is obtained directly from irradiation test data and is correlated using a specific model of hot pressing of the fuel. In the CYGRO code, fuel plasticity is calculated from UO_2 creep data (including fission rate effects) and applied with the same hot pressing relationship used in the OLYMPUS Code.

THE OLYMPUS CODE

GENERAL

The OLYMPUS code utilizes a phenomenological model of fuel pin performance in which experimental observations are linked with basic descriptions of known phenomena. The model is correlated with the data to enable reproduction of the experimental observations. The model was developed from detailed analysis of experimental irradiation tests performed on stainless steel clad, mixed oxide fuel pins, irradiated in DFR and EBR-II. The basic fuel pin performance model illustrated in Figure 3 was formulated, using the results of the analysis of the irradiation data together with cladding swelling information. The four basic phenomena considered by the model are stainless steel swelling, cladding creep, fuel swelling, and hot pressing of the fuel by the stresses imposed by the cladding after fuel-cladding interaction has occurred. A "critical burnup" (B*) is defined. For burnups less than B*, the total cladding strain (% $\Delta D/D)T$ is essentially due to stainless steel swelling. The stresses created by fuel/cladding interaction result in hot-pressing of the fuel into as-fabricated porosity, and cause only a small amount of cladding creep strain. At B* all available porosity in the system is exhausted and the cladding deforms at a rate equal to the radial fuel swelling rate. The basic model is expressed by the following equations:

$$\left(\% \frac{\Delta D}{D}\right)_{Total} = 1/3\ [\text{Clad Swelling, } (\%\Delta V/V)_s] + [\text{Clad Creep, } (\%\Delta D/D)_c] \quad (5)$$

[c] Discussed further with OLYMPUS Code.

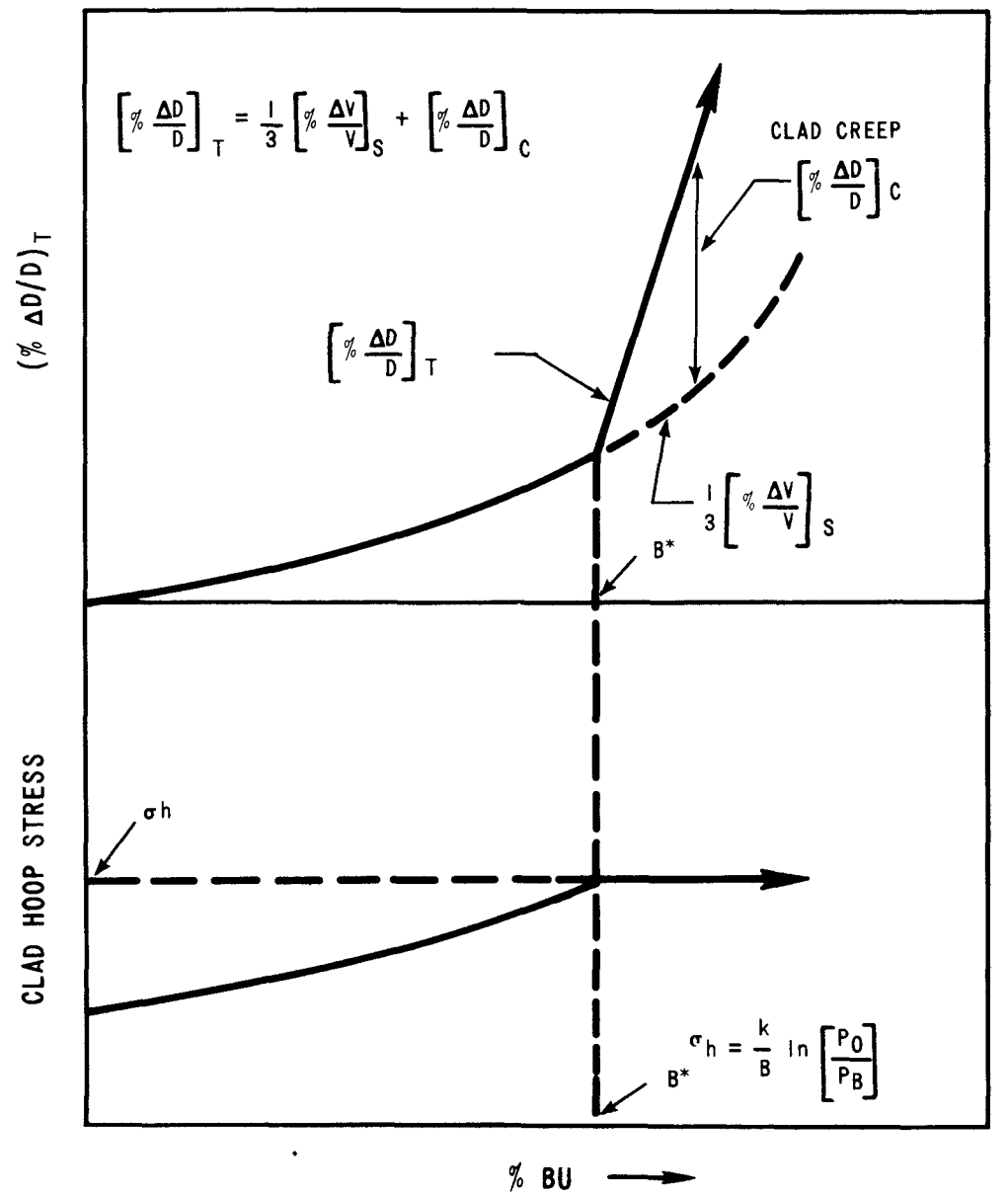

Figure 3. Illustration of the OLYMPUS-1 Fuel Pin Performance Model

3469-3

The definition of the critical burnup, B* (atom percent) is given by:

Below B*

$$(\%\Delta D/D)_T = 1/3\ (\%\Delta V/V)_s \tag{6}$$

Above B*

$$(\%\Delta D/D)_T = 1/3\ (\%\Delta V/V)_s + (\%\Delta D/D)_c \tag{7}$$

$$(\%\Delta D/D)_C = 1/2\ (B - B^*)\ [(\%\dot{\Delta V}/V)_F - (\%\dot{\Delta V}/V)_S] \tag{8}$$

where $(\%\dot{\Delta V}/V)_F$ and $(\%\dot{\Delta V}/V)_S$ are the fuel and cladding swelling rates per % BU, respectively.

The fuel swelling rate is given by:

$$(\%\dot{\Delta V}/V)_F = 2\ (\%\dot{\Delta D}/D)_T + (\%\dot{\Delta L}/L) \tag{9}$$

Irradiation data indicate that axial pin extension appears to be controlled by cladding swelling. Thus:

$$(\%\dot{\Delta L}/L) = 1/3\ (\%\dot{\Delta V}/V)_S \tag{10}$$

The DFR and EBR-II irradiation data indicate that $(\%\dot{\Delta D}/D)_T$ is approximately 0.6% $\Delta D/D$/% BU above B* with linear power (Q) between 8-15 kw/ft, fluence/BU ratio approximately 8×10^{21}/% BU and mean cladding temperature 400-650°C. Thus, $(\%\dot{\Delta V}/V)_F = 1.2\% + 1/3\ (\%\dot{\Delta V}/V)_S$, and from EBR-II and DFR fluence/burnup ratios, $(\%\dot{\Delta V}/V)_F = 1/3\%$ per % BU.

A simplified version of the hot pressing equation derived by Murray, et.al.,[12] is used to yield the relation:

$$\sigma_h = k/B\ \ln\ (P_0/P_B) \tag{11}$$

where

σ_h is the clad hoop stress

P_0 is the initial porosity (100 - hot smear density)

P_B is the porosity at burnup B

k is a constant related to the plasticity of the fuel

$P_B = P_0$ - Fuel Swelling + Clad Swelling

Therefore

$$P_B = P_0 - (\%\Delta\dot{V}/V)_F \, B + (\%\Delta V/V)_S \qquad (12)$$

The critical burnup B*, obtained from Equation (11), is achieved when the cladding hoop stress, σ_h attains the value required to give a cladding creep rate equal to the radial fuel swelling rate.

The values of B* and P_o are obtained from the experimental irradiation tests, σ_h determined from cladding creep data, and P_B is computed from Equation (12). Correlation of Equation (11) and experimental data provides k values for particular combinations of rod power level and mean cladding temperatures.

The OLYMPUS model was recently revised to include a description of the phenomena occurring in a fuel pin during the closure of the pellet-cladding gap. This involves calculating the change in gap size during startup as a consequence of the differential thermal expansion of fuel and cladding. Once fuel/cladding contact occurs, the hoop stress in the cladding is computed using a modified form of Equation (11). In the revised code, the creep strain arising from these stresses is calculated. Consequently, the revised model computes the small amount of cladding creep strain preceeding the attainment of the critical burnup.

Figure 4 illustrates the manner in which cladding hoop stress develops as a function of burnup in this revised model. Figure 4(a) shows the stress accumulation when stainless steel swelling is comparatively small, such as occurs in the case of pins operating at low fluence/burnup ratios (e.g. EBR-II and DFR fully enriched pins), or high fluence/burnup ratios such as FFTF pins operating with low cladding temperatures. Figure 4(b) shows the behavior of the hoop stress when stainless steel swelling is large as in the case of high fluence/burnup pins operating with cladding temperatures greater than 450°C. In these latter cases the cladding swelling rate is initially relatively small, but as it follows a $(\phi t)^{1.7}$ relationship, at high fluences the difference between fuel and cladding swelling decreases rapidly so that the cladding hop stress is found to decrease with burnup.

Studies utilizing the above simple form of OLYMPUS are labeled the OLYMPUS-I series with letters A, B, C, and D to define the specific stainless steel swelling equations used. A second generation of codes (OLYMPUS-II) based on similar principles is now under development. The OLYMPUS-II codes include the following new features:

1. The fuel swelling rate, Equation (9), is being redefined as a function of fuel surface temperature and linear power level.

2. The hot pressing equation is being evaluated incrementally with burnup.

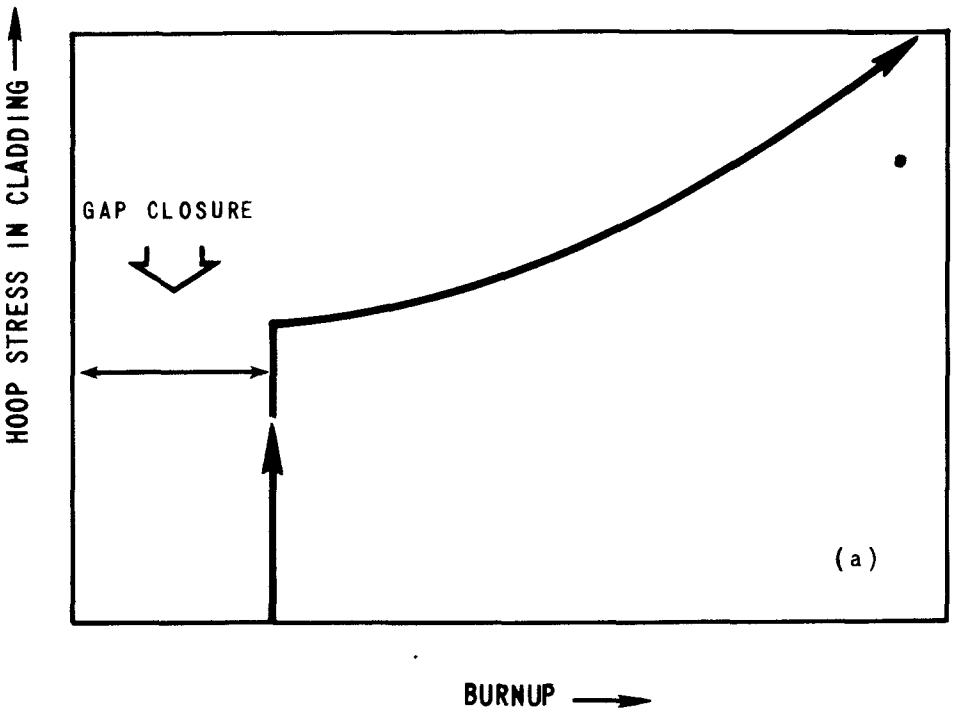

(a) Low Stainless Steel Swelling Rate

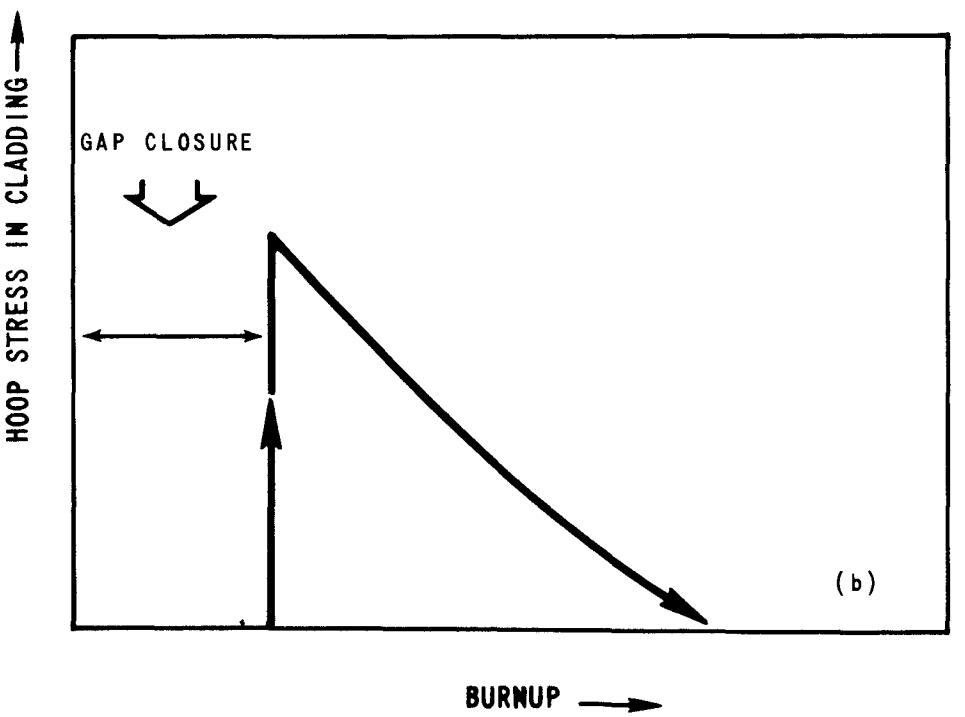

(b) High Stainless Steel Swelling Rate

Figure 4. Illustration of Cladding Hoop Stress in Revised OLYMPUS-I Model

3469-4

3. Irradiation induced creep of stainless steel is being added.

4. Additional sources of cladding strain below the critical burnup (including thermal stress and fission gas pressure) are being added.

OLYMPUS CODE RESULTS

The OLYMPUS code was applied to the conceptual design of FFTF fuel pins to define a maximum fuel smear density that would meet the design requirements. The reference design for the first FFTF core requires that the cladding mechanical strain (exclusive of cladding swelling) be less than 0.2% in any fuel pin up to the target maximum burnup of 80,000 MWd/Te. The design requirement can be achieved if the superimposed fuel swelling, fission gas pressure, and thermal strain at any axial location in any pin is less than 0.2%. Analysis of the fission gas pressure strains revealed that cladding mechanical strains (including thermal strain) were less than 0.2% at the hottest region of any pin (650°C in the axial blanket region of a hot channel pin) if the end-of-life plenum gas pressure does not exceed 772 psi (effective cladding hoop stress of 7,600 psi assuming minimum cladding thickness of 10 mils vs the nominal 15 mil wall).

The OLYMPUS code was used to compute the total creep strain due to the superposition of fuel/cladding mechanical interaction, fission gas pressure, and thermal strain. The results indicated that the total creep strain at any axial location in any pin was less than 0.2% strain for a maximum fuel smear density of 88% TD and a nominal diametral gap of 6 mils. Illustrations of several of the computer results are presented below.

Figures 5 and 6 show the predicted end-of-life (80,000 MWd/Te peak burnup) axial $(\Delta D/D)_T$ profiles for a "hot channel" and "average channel" pin with an effective cladding thickness of 10 mils at several values of fuel smear density. The results obtained, using the mean values of stainless steel swelling, given by Equation (2), show that the cladding strain is controlled by stainless steel swelling when the fuel smear density (ρ_{sm}) is less than 90% TD (theoretical density). Similar analysis using the lower boundary of the 95% confidence of the swelling equation for any one pin (prediction interval for next observation) shows that cladding strain is controlled by stainless steel swelling when the fuel smear density is less than 89% TD. Thus, specification of a maximum fuel smear density of 88% TD is consistent with the OLYMPUS prediction that the critical burnup will not be exceeded anywhere within the FFTF core.

Figures 7 and 8 illustrate detailed OLYMPUS predictions of the cladding hoop stress resulting from fuel/cladding mechanical interaction below the critical burnup. Also shown in Figures 7 and 8 is the hoop stress due to fission gas pressure. Figure 7 shows that the incremental stress due to fuel/cladding mechanical interaction is under 16,000 psi for fuel smear densities of both 88 and 90% TD. The incremental strain due to fuel/cladding mechanical interaction (for ρ_{sm} = 88% TD) is small. The total strain (elastic and creep) computed for the midplane of the "hot channel" pin (520°C, 970°F) is 0.15% of which 0.07% is thermal strain, 0.05% is elastic strain, and the remainder primary and secondary creep strain. Figure 8 shows a

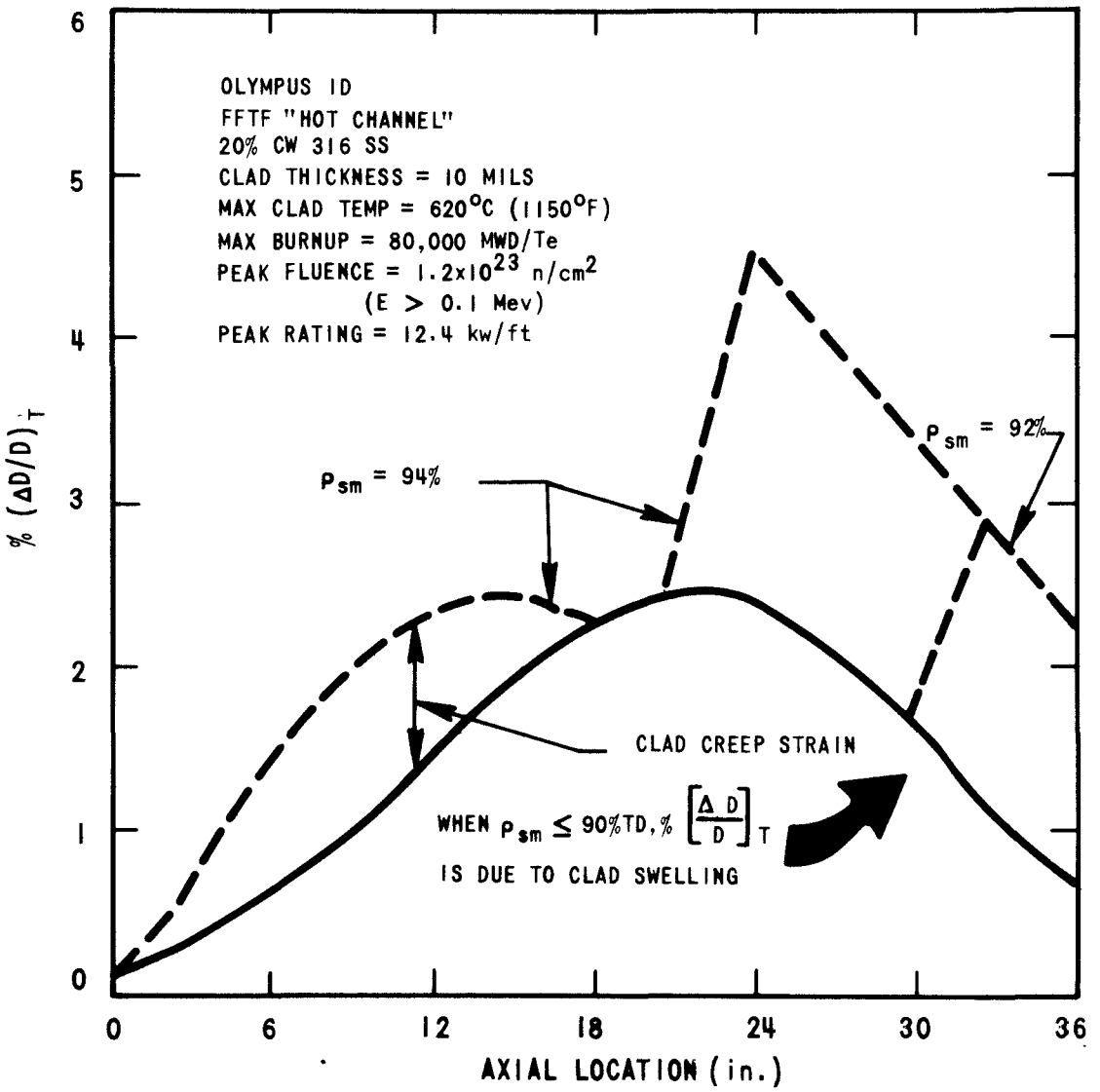

Figure 5. Total Cladding Strain for an FFTF "Hot Channel" Pin as a Function of Axial Location and Fuel Smear Density.

3469-5

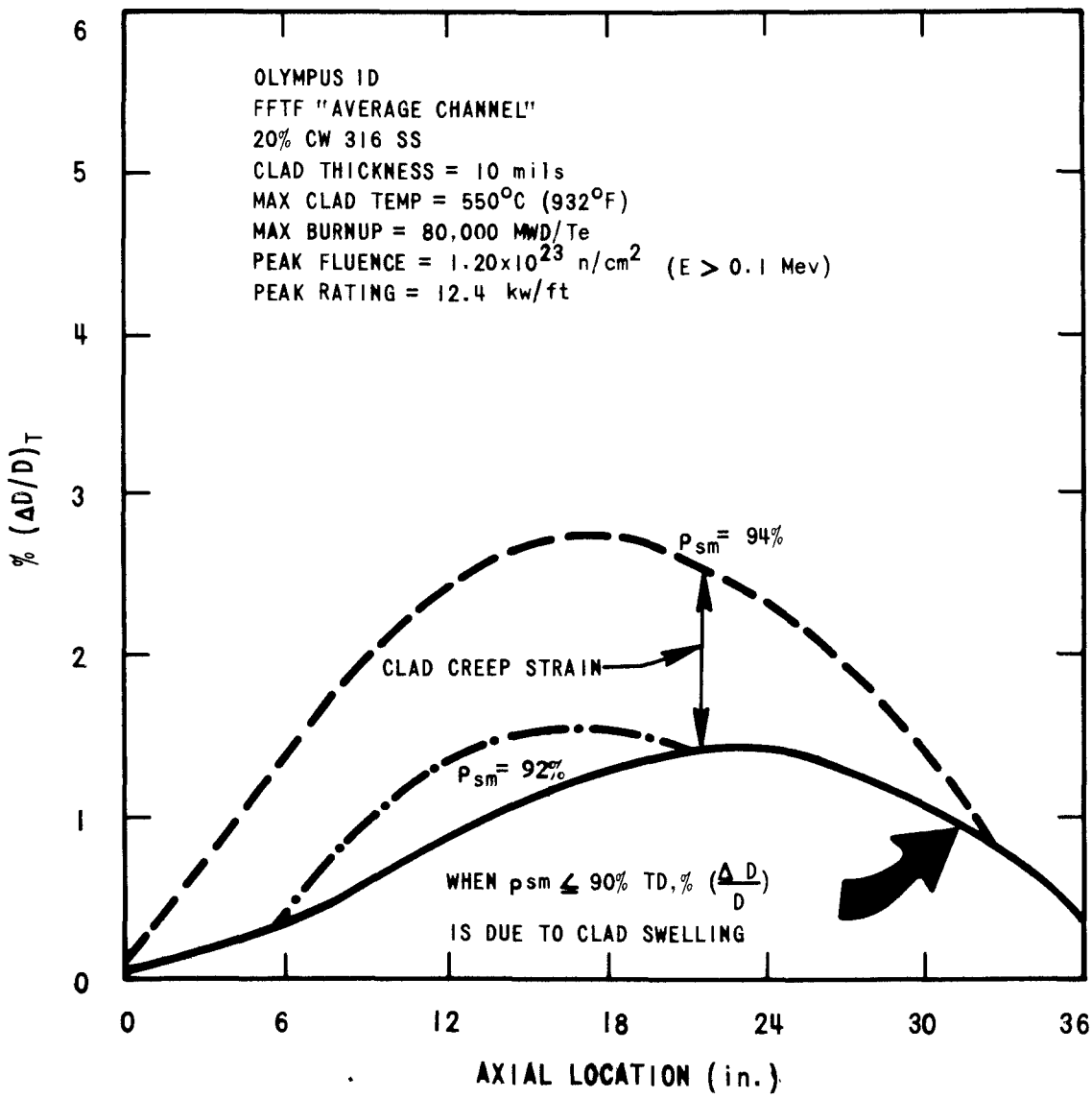

Figure 6. Total Cladding Strain for an FFTF "Average Channel" Pin as a Function of Axial Location and Fuel Smear Density.

3469-6

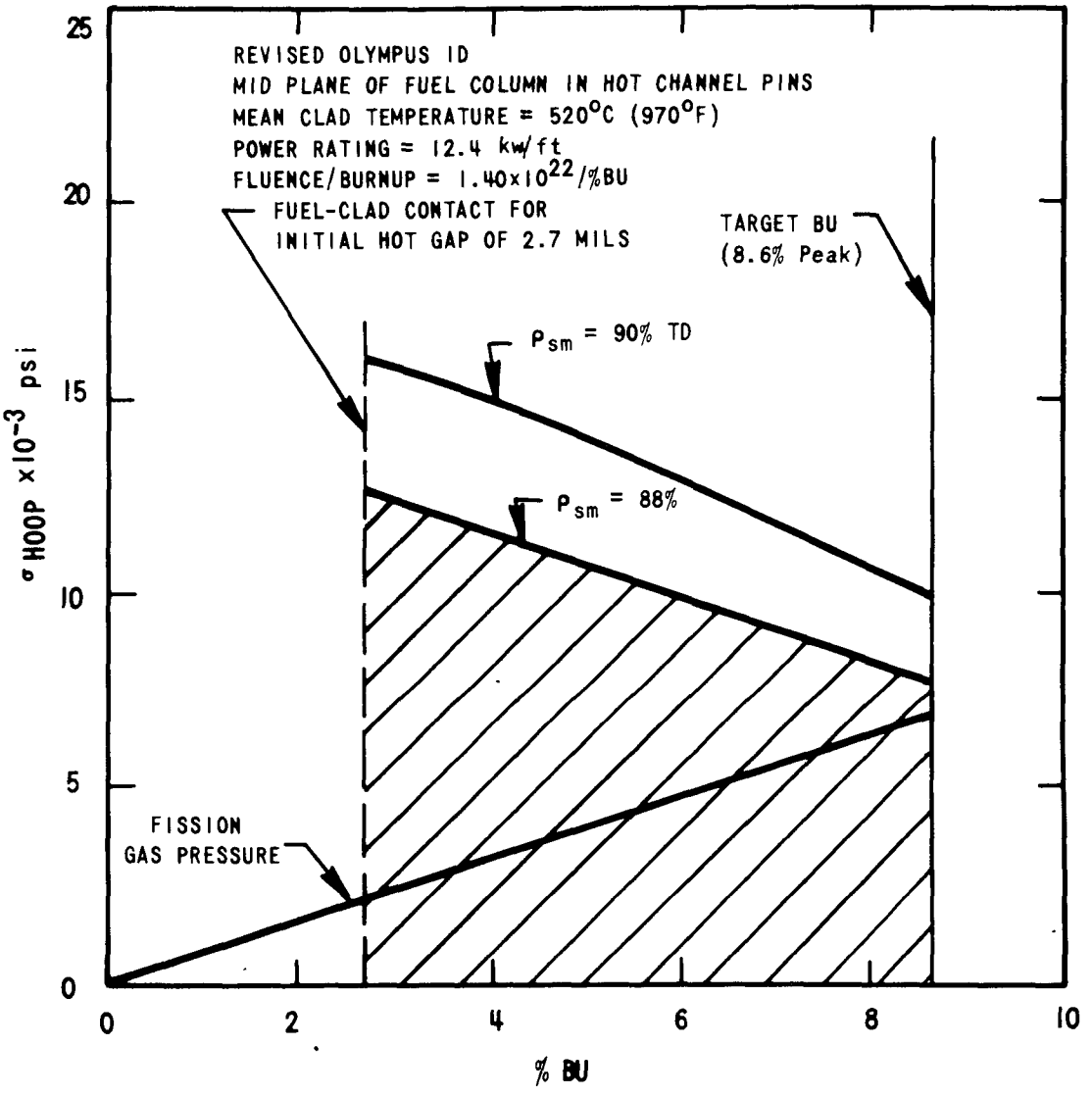

Figure 7. Cladding Hoop Stress in a "Hot Channel" Pin at the Reactor Mid-Plane Position (20% CW 316 SS)

3469-7

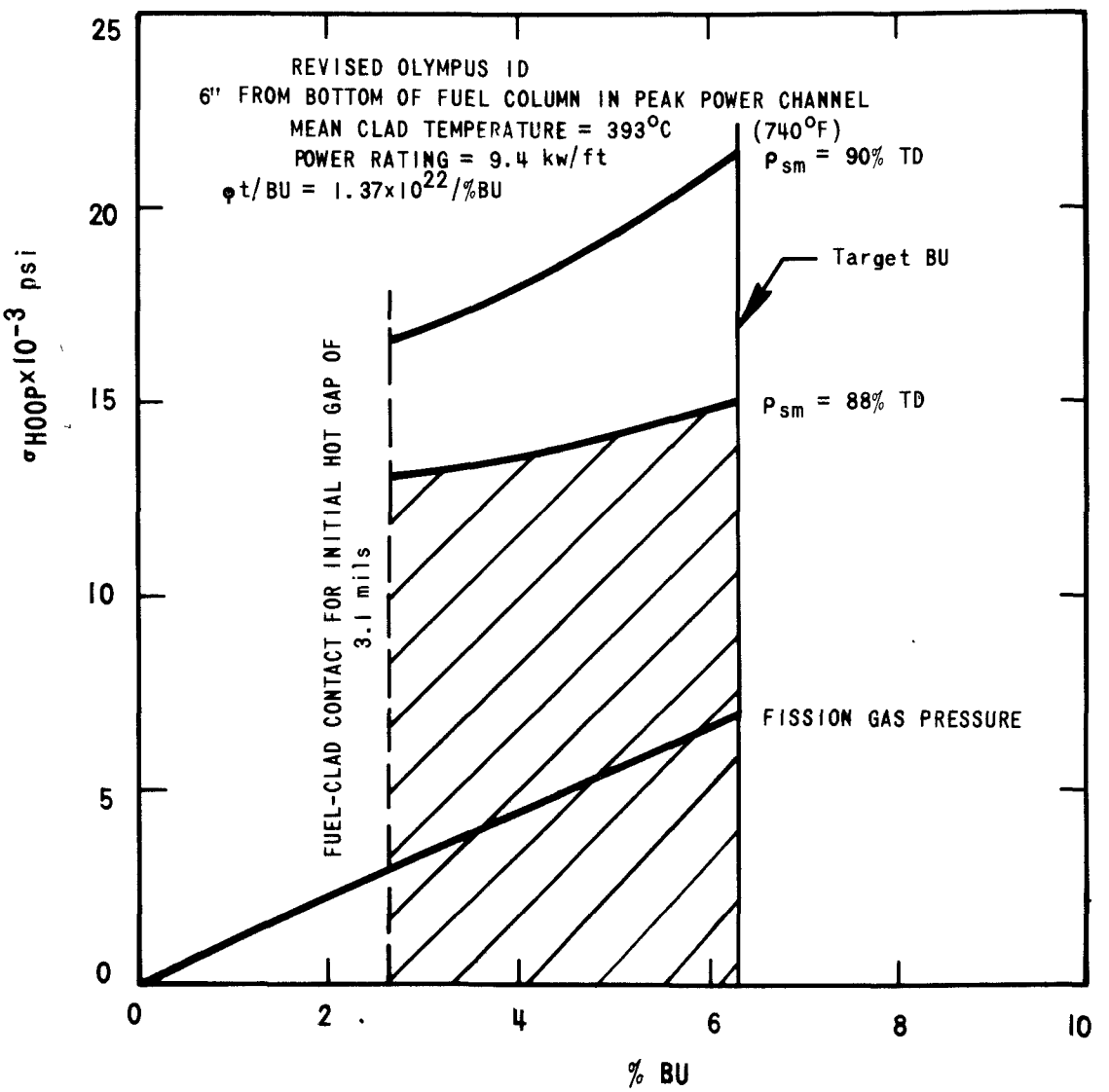

Figure 8. Cladding Hoop Stress in a "Peak Power Channel" Pin at Six Inches from the Bottom of the Fuel Column

3469 -8

cladding hoop stress of about 14,000 psi at 393°C (740°F) for a fuel smear density of 88% TD for a "peak power channel." The total strain computed for the cold region of a "peak power channel" is 0.11% of which 0.05% is thermal strain 0.05% elastic strain, and the remainder primary and secondary creep strain.

The OLYMPUS code was used to evaluate the total strain along the length of FFTF fuel pins operating under "hot channel," "peak channel," and "average channel" conditions[d]. In all cases, the total strain was less than 0.2% when the maximum fuel smear density was 88% TD.

THE CYGRO-2 CODE

GENERAL

The CYGRO-2 code is a digital computer program which permits calculation of stresses and strains in a cross section of fuel and cladding undergoing thermal expansion and irradiation growth.[2] Current activities are directed toward the application of CYGRO-2 for fast reactor fuel rod performance analysis. The original CYGRO-2 code has been modified in the following ways.

1. The thermal and gap conductivity calculations have been replaced by a FIGRO[13] type of analysis.

2. The thermal creep and irradiation-induced swelling of Type 316 (both solution treated and 20% cold worked) stainless steels are now options in the code.

3. Empirical fuel swelling models are also available options in addition to the modified Greenwood-Speight[10] model in the code.

The empirical fuel swelling models used in the present analysis are shown in Figure 9.

As mentioned earlier, the CYGRO code for fast reactor applications (called CYGRO-F) is involved in a sensitivity analysis study. Prior to initiation of this complete sensitivity study, a limited evaluation was made of CYGRO-F at fast reactor operating conditions.

PRELIMINARY CYGRO-F RESULTS

The parameters used in this study are given in Table 2. The principal variables were pellet type, power level, and fluence/burnup ratio. A limited study was also made using FFTF fuel operating parameters.

---

[d] The FFTF parameters examined are defined on Figures 5-8. The cases considered involve axial cladding temperature variations superimposed on peak flux and power profiles.

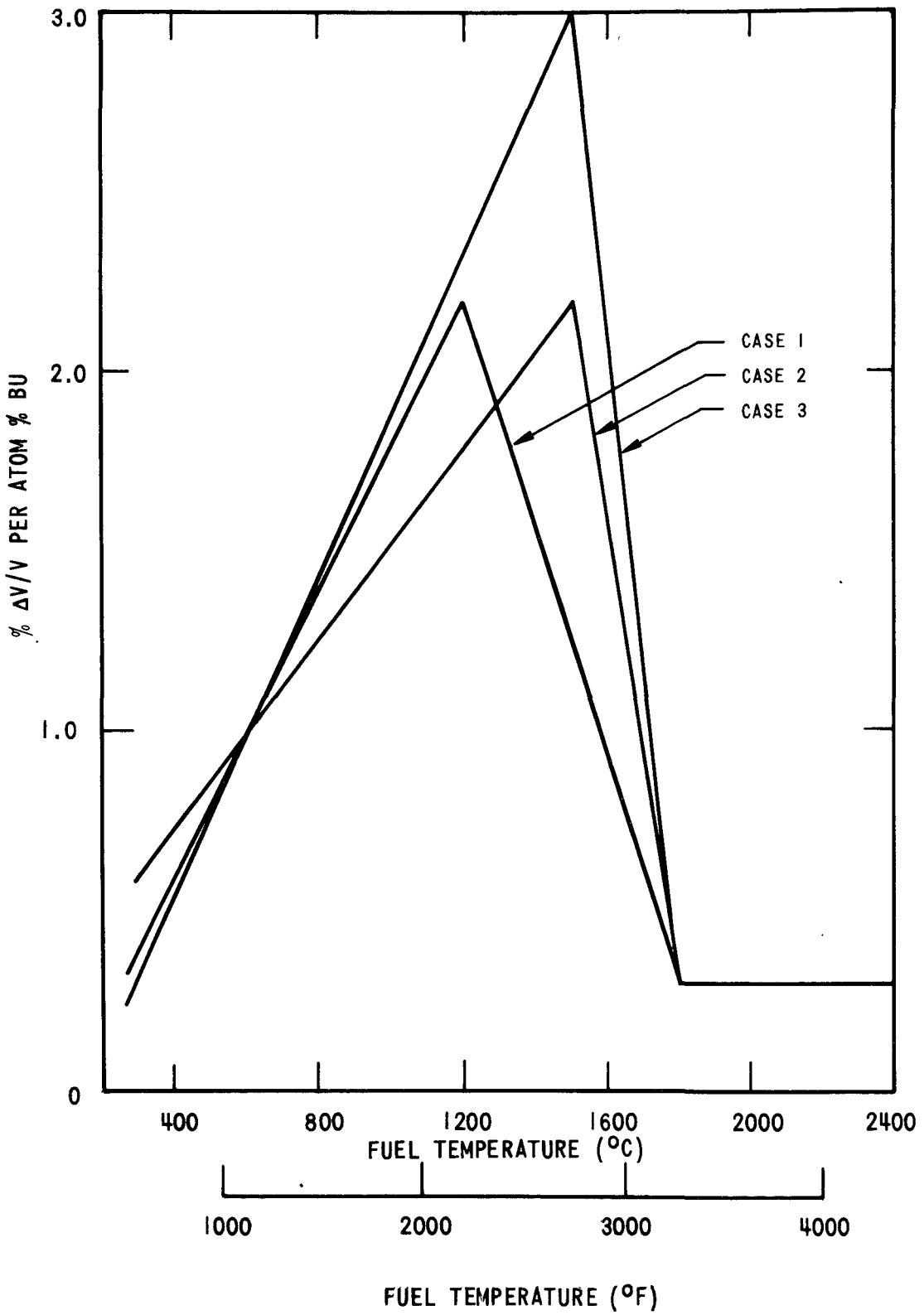

Figure 9. Empirical Fuel Swelling Models Used in CYGRO-F Code.

3469-9

Table 2. Parameter Selection for Preliminary CYGRO-F Studies (Cladding is 20% Cold Worked Type 316)

FUEL PELLET PARAMETERS (SOLID AND ANNULAR)

Pellet Type	% Smear Density	% Pellet Density	Diametral Gap, mils	Fuel OD (in.)	Fuel ID (in.)
Annular	82	93.7	5	0.217	0.060
Solid	82	86	5	0.217	--

FUEL ROD OPERATING PARAMETERS[e]
Fast Flux (E > 0.1 Mev) of 10^{15} and 5 x 10^{15} n/cm^2 sec

Linear Power (kw/ft)	Specific Power (w/gm)	Time to 1 a/o BU (hr)	Fluence/Burnup Ratio (10^{21} n/cm^2 per % BU)	
			Low Flux	High Flux
9	128	1740	6.2	-
12	171	1310	4.2	20
15	214	1050	3.8	-

[e]Mean clad temperature of 555°C (1030°F)

Figure 10 illustrates the CYGRO-F outputs for the case of a solid pellet at 12 kw/ft for the three empirical swelling models. The remainder of the study utilized the Case #3 swelling model. Figures 11 and 12 show the total cladding strain for solid and annular pellets at 9, 12 and 15 kw/ft. The cladding swelling shown is for 12 kw/ft; i.e. fluence/burnup ratio of 4.2 x 10^{21} n/cm^2 per %BU. Comparison of Figures 11 and 12 reveal a lower total cladding strain for solid pellets (pellet density of 86% TD) than for annular pellets (pellet density of 93.7% TD) at the same smear density (82% TD). Figures 13 and 14 illustrate the variation in total porosity (initial fabricated porosity less restructuring plus fuel swelling) and the remaining as-fabricated porosity (initial porosity less restructuring) as functions of fuel radius and burnup. The lower total cladding strain for solid versus annular pelleted fuel rods is related to the greater as-fabricated porosity in the low density solid pellets. Figures 13 and 14 also show the radial variation in fuel swelling by the difference between the total porosity and the fabrication porosity. Figure 15 shows the variation in center hole size as a function of burnup for both solid and annular pellets.

The CYGRO-F comparison of solid and annular pellets shows a lower cladding creep strain with solid pellets at the low fluence/burnup ratios typical of test reactors. Similar studies are planned at the high fluence/burnup ratios of the LMFBR. CYGRO-F was also used to examine several selected cases of FFTF fuel rod operating parameters. Several important results were obtained from this study. At the core centerline, stainless swelling is comparable

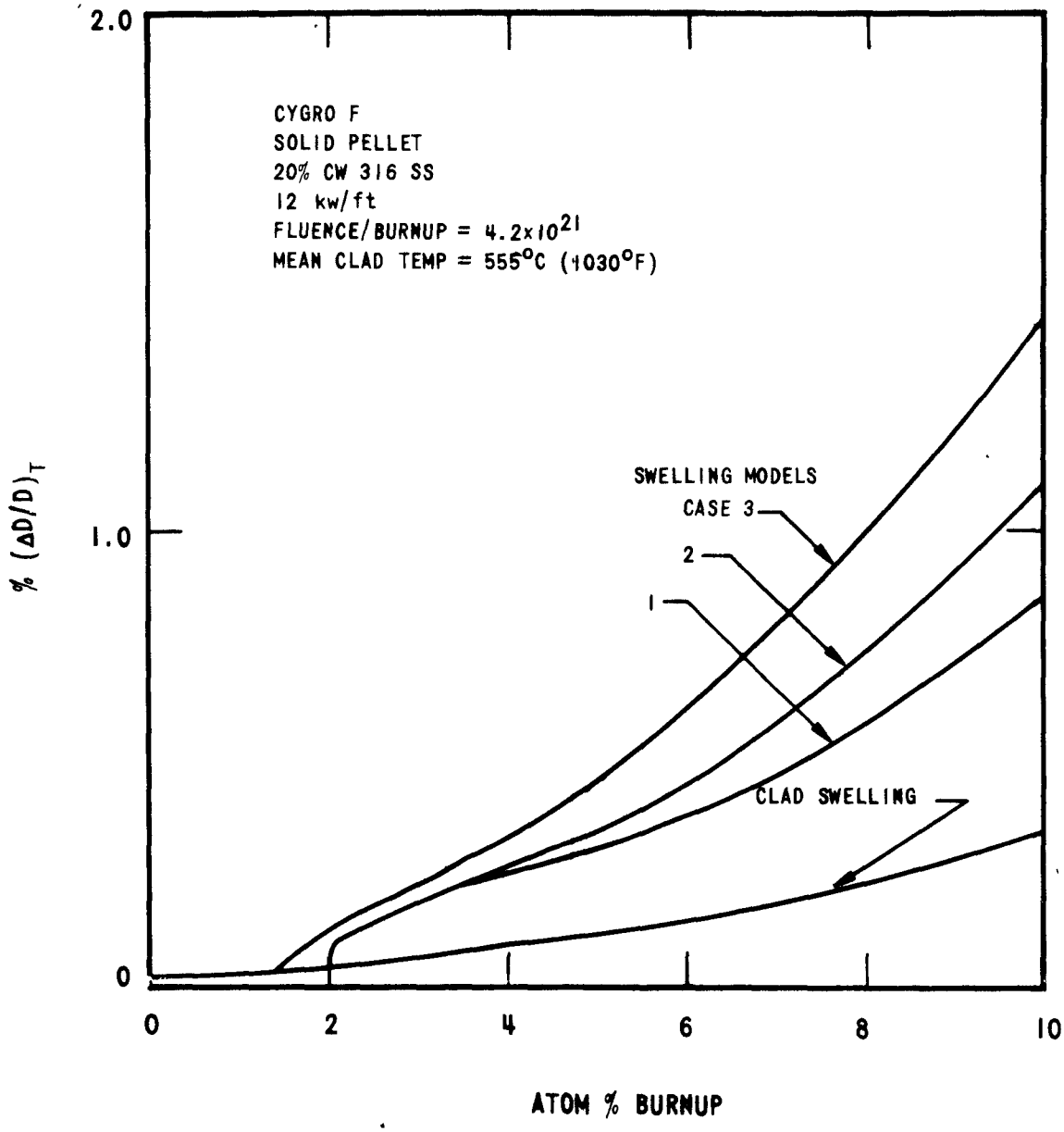

Figure 10. Total Cladding Strain Given by CYGRO-F Code as a Function of Burnup and Swelling Model.

3469-10

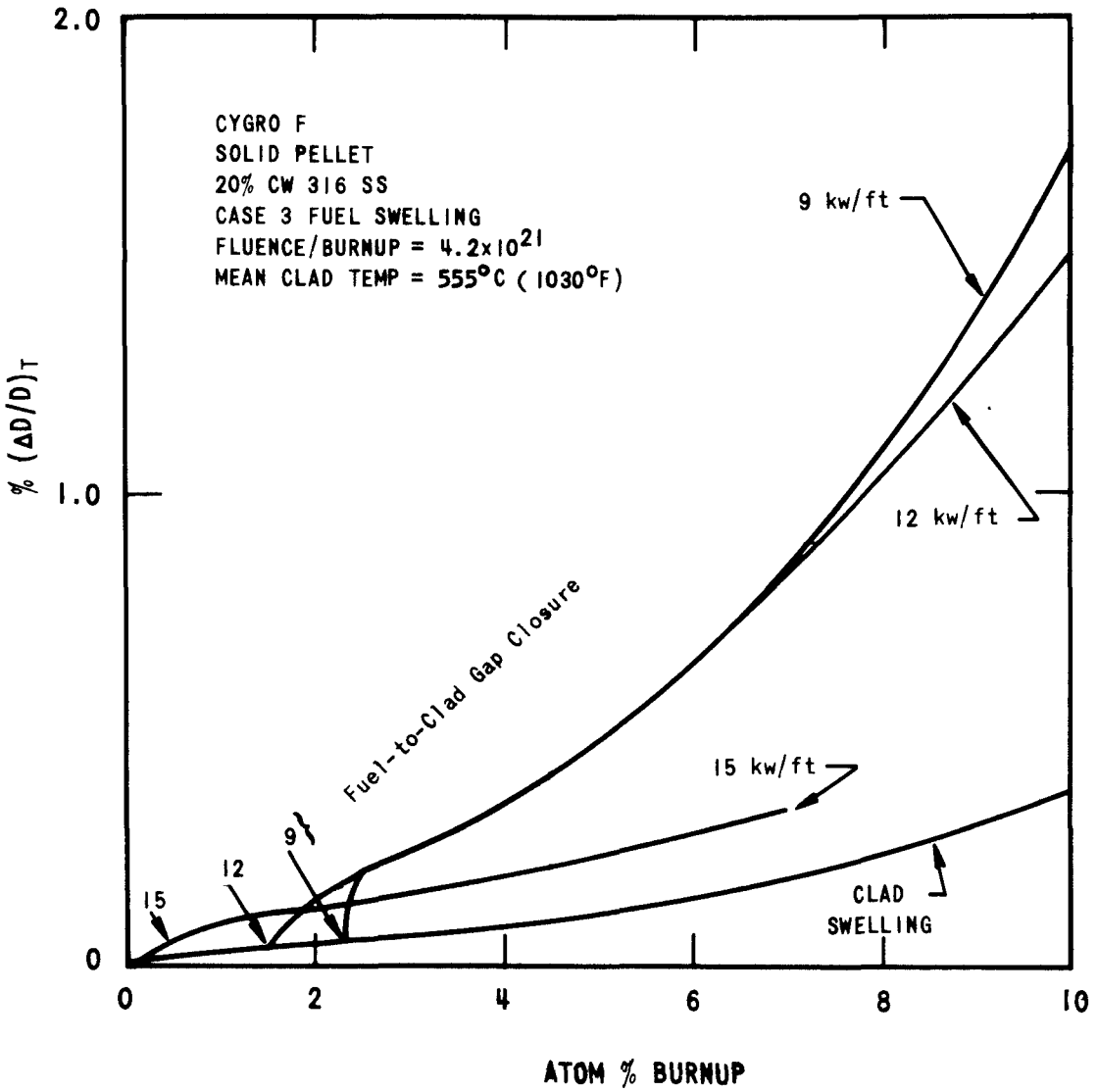

Figure 11. Total Cladding Strain Given by CYGRO-F Code for a Solid Pellet (P_{sm} = 82% TD) as a Function of Burnup and Power Level.

3469-11

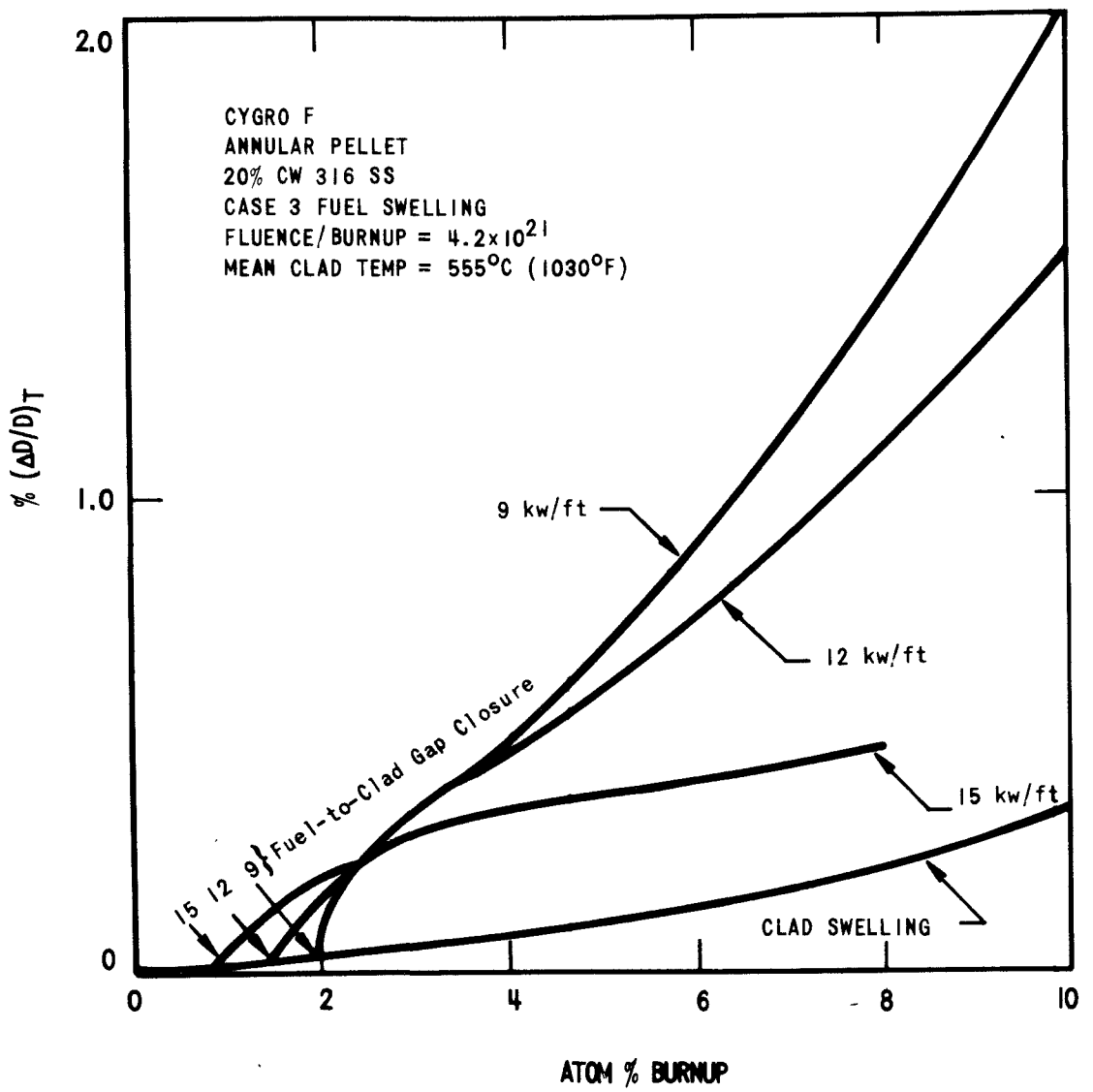

Figure 12. Total Cladding Strain Given by CYGRO-F Code for an Annular Pellet (ρ_{sm} = 82% TD) as a Function of Burnup and Power Level.

3469-12

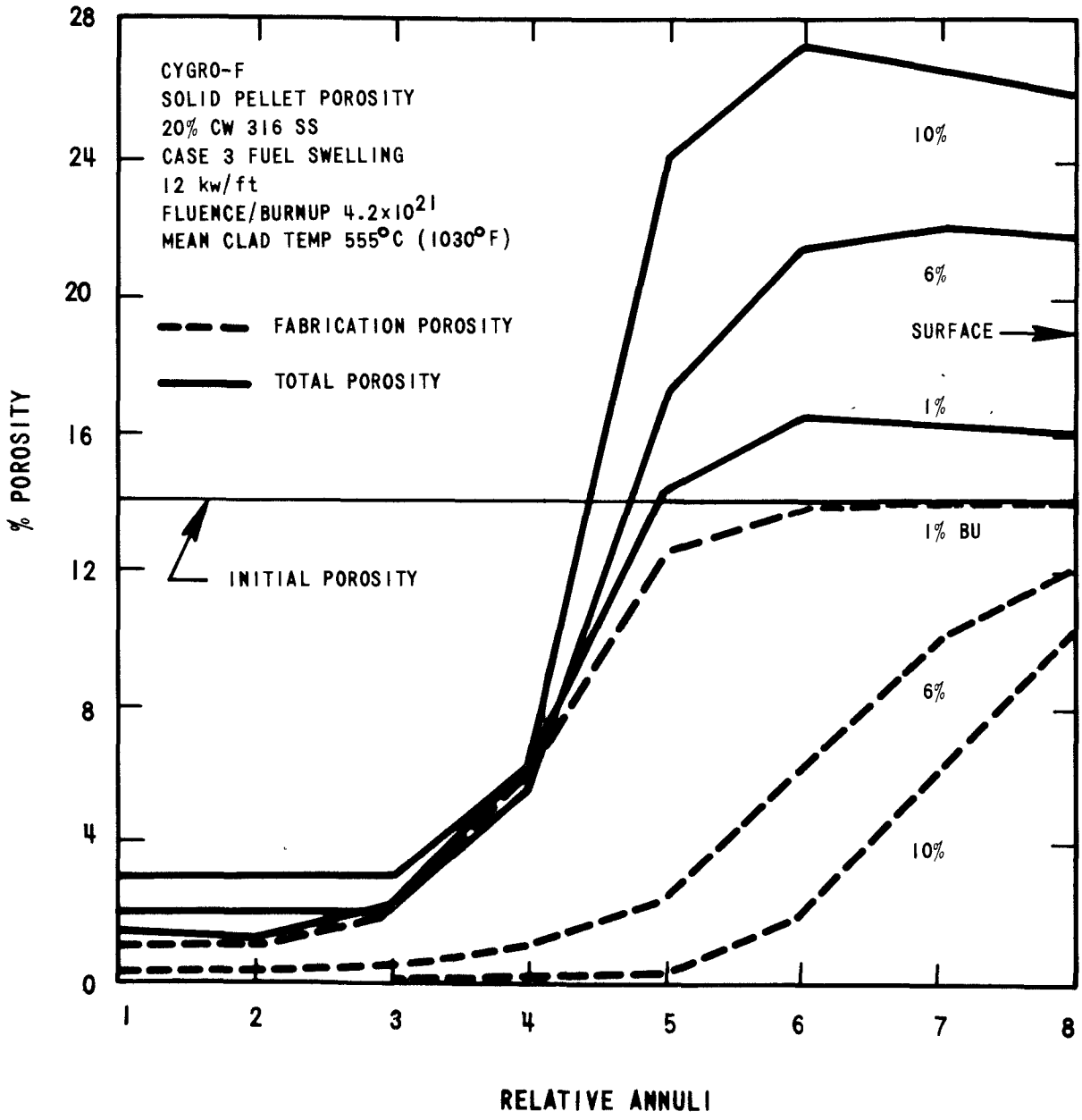

Figure 13. Variation of Porosity in a Solid Pellet (ρ_{sm} = 82% TD) with Radial Position and Burnup.

3469-13

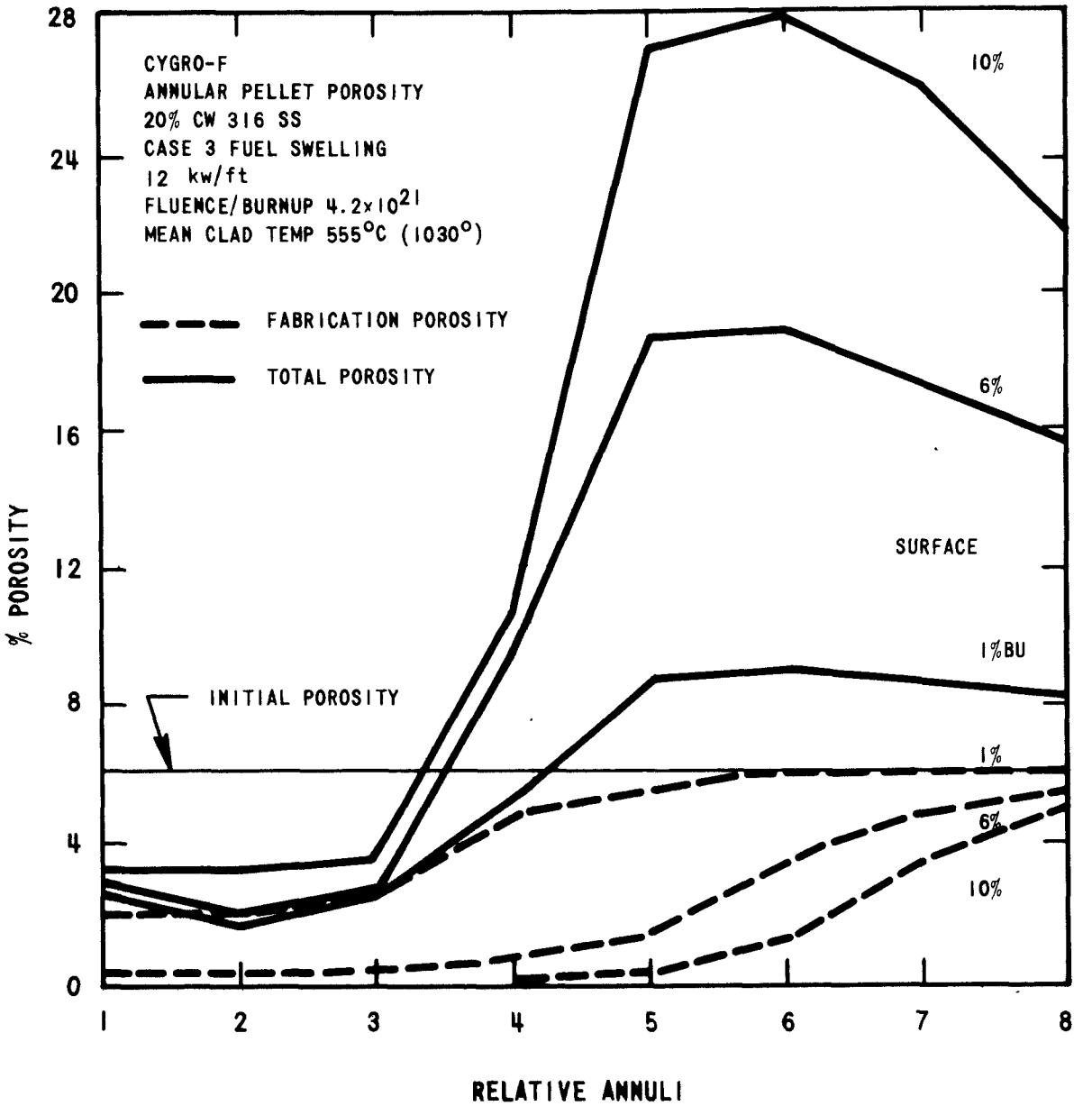

Figure 14. Variation of Porosity in an Annular Pellet (ρ_{sm} = 82% TD) with Radial Position and Burnup.

3469-14

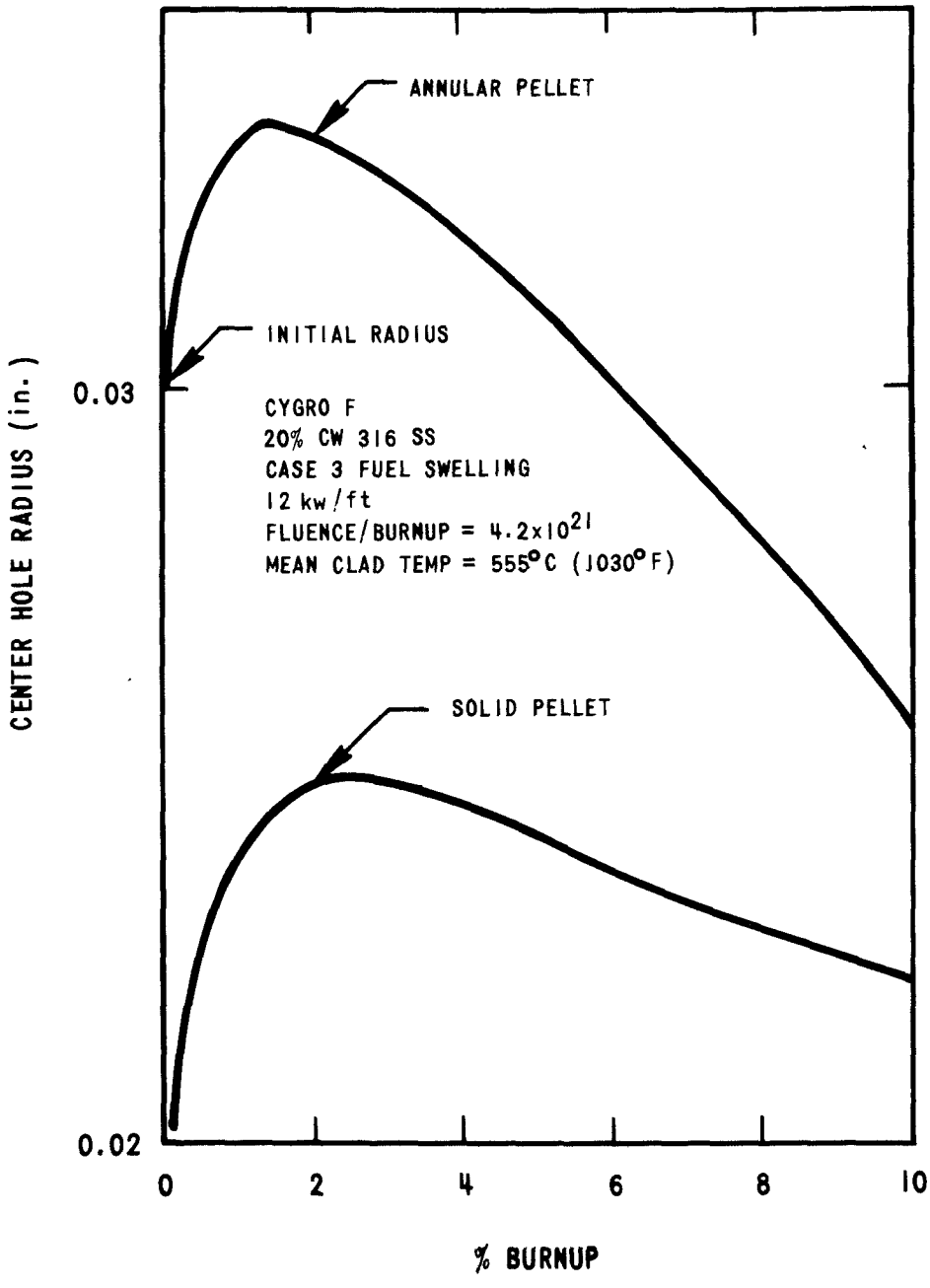

Figure 15. Variation in Center Hole Radius with Burnup for a Solid and Annular Pellet (ρ_{sm} = 82% TD).

3469-15

to the presently selected values of fuel swelling. In this case, CYGRO-F predicts a minimum fuel/cladding gap at about 5% BU followed by an increasing gap with burnup, resulting in increases in fuel centerline temperature. The fuel centerline temperatures, given by the present model, are considered to be overestimated. It is expected that the development of a combined fuel cracking, crack displacement, and crack healing model would provide fuel/cladding contact at low burnup or a minimum fuel/cladding gap. Further analytical work on a detailed gap behavior model is planned.

Another interesting result occurs in the cladding due to differential stainless steel swelling across the cladding wall. Differential cladding swelling adds significant tensile (outer fibers) and compressive (inner fibers) hoop stress to the cladding. For example, at 455°C (850°F) and 6% BU the hoop stress (and shear stress) is 28,000 psi. The stress is achieved despite simultaneous thermal stress relaxation. Further study is planned utilizing the available irradiation creep models.

Finally, several direct comparisons were made of OLYMPUS and CYGRO-F output at FFTF conditions. In all cases at a smear density of 88% TD the overall results and conclusions were similar. Some differences were noted in levels of cladding hoop stress at low cladding temperatures. For example, the CYGRO-F prediction for the parameters defined in Figure 8 indicate a fuel/cladding mechanical interaction hoop stress initiating at about 4% BU and a stress of 28,000 psi at 6% BU. The total plastic strain given by CYGRO-F at 6% BU is less than 0.01%. Further detailed comparisons of OLYMPUS and CYGRO-F are planned after completion of the CYGRO-F sensitivity analysis.

SUMMARY AND CONCLUSIONS

The status of fuel performance model development work involving the OLYMPUS and CYGRO-F codes has been reviewed in this report. The status of several critical areas involving required experimental data was covered and current input quantities were defined. The outputs from the codes were illustrated by parametric studies and specific application to FFTF fuel rod performance analysis. The studies indicated the major effects of stainless steel swelling on fuel rod performance and the relationship between fuel density and cladding creep strain.

This review of fuel performance model development shows the applicability of the OLYMPUS and CYGRO-F codes to LMFBR fuel rod design. The results indicate that the codes can aid greatly in the definition of critical experimental irradiation programs. In particular, WARD is fabricating subassemblies for irradiation in EBR-II to evaluate specific features of the performance codes.

ACKNOWLEDGMENTS

The authors wish to acknowledge the work of B. L. Harbourne, W. K. Appleby, and M. S. Beck of the Westinghouse Advanced Reactors Division who are actively involved in the development of the OLYMPUS and CYGRO-F codes.

REFERENCES

1. Westinghouse Advanced Reactors Divison Quarterly Reports

   WARD-3791-37 (For period ending March 31, 1969)
   WARD-3791-39 (For period ending June 30, 1969)
   WARD-4135-1 (For period ending September 30, 1969)

2. C. M. Friedrich and W. H. Guilinger, Bettis Atomic Power Laboratory Report, WAPD-TM-547 (1966).

3. E. Duncombe, J. E. Meyer, W. A. Coffman, Bettis Atomic Power Laboratory Report, WAPD-TM-583 (1966).

4. K. R. Merkx, Nucleonics, Vol. 25, p. 67 (1967).

5. Interim Agreement on Stainless Steel Swelling Equations, Battelle Northwest Laboratory and Westinghouse Advanced Reactors Division, (August 1969).

6. G. W. Lewthwaite, D. Mosedale and I. R. Ward, Nature, Vol. 216, p. 472 (1967).

7. R. V. Hesketh, "Proceedings International Conference Solid State Physics Research with Accelerators," Brookhaven National Laboratory Report, BNL 500.83, p. 389, (1968).

8. F. A. Nichols, Bettis Atomic Power Laboratory Report, (Presented at AIME Meeting), October 1969, WAPD-T-2252 (1969).

9. W. E. Baily, R. C. Nelson, B. F. Rubin, and C. N. Spalaris, ANS Transactions Vol. 11, p. 515 (1968).

10. H. Lawton, K. Q. Bagley, E. Edmonds, and H. E. Tilbe, Fast Breeder Reactors (Proceedings of the London Conference) p. 631 (May 1966).

11. J. Standring, I. P. Bell, H. Tickle, and A Glendenning, UKAEA Report, (Presented at ASTM Meeting, June 1968), TRG Report 1789 (1969).

12. P. Murray, D. T. Livey, and J. Williams, Ceramic Fabrication Processes, W. D. Kingery, Editor, John Wiley and Sons, Inc., New York (1958).

13. I. Goldberg, L L. Lynn, and C. D. Sphar, Bettis Atomic Power Laboratory Report, WAPD-TM-618 (1966). See also Addendem I (1967).

14. G. W. Greenwood and M. V. Speight, Jnl. Nuclear Materials, Vol. 10, p. 140 (1963).

EXTERNAL DISTRIBUTION LIST

U. S. ATOMIC ENERGY COMMISSION

Division of Reactor Development and Technology
Washington, D. C. 20545

Assistant Director, Engineering Standards
Assistant Director, Nuclear Safety
Assistant Director, Plant Engineering
Assistant Director, Program Analysis
Assistant Director, Project Management (2)
Assistant Director, Reactor Engineering (2)
Assistant Director, Reactor Technology
Chief, Fuels and Materials Branch (3)
Chief, Fuel Engineering Branch
Chief, Reactor Vessels Branch

Division of Naval Reactors
Chief, Nuclear Materials Branch
United States Atomic Energy Commission
Washington, D. C. 20545

New York Operations Office
Manager (2)
U. S. Atomic Energy Commission
376 Hudson Street
New York, New York 10014

Division of Technical Information Extension (3)* (50)**
United States Atomic Energy Commission
P. O. Box 62
Oak Ridge, Tennessee 37831

Office of Assistant General Council for Patents
U. S. Atomic Energy Commission
Washington, D. C. 20545

Assistant Director Pacific Northwest Laboratory
U. S. Atomic Energy Commission
P. O. Box 550
Richland, Washington 99352

AEC-RDT Site Offices
Argonne National Laboratory
U. S. Atomic Energy Commission
Building 2
Argonne, Illinois 60439

---

* Submitted with transmittal form AEC-426

** Submitted for transmittal to recipient under UKAEA/USAEC and EURATOM/USAEC Fast Breeder Reactor Information Exchange Arrangements

Argonne National Laboratory
U. S. Atomic Energy Commission
P. O. Box 2108
Idaho Falls, Idaho 83401

Atomics International
U. S. Atomic Energy Commission
P. O. Box 1446
Canoga Park, California 91304

General Electric Company, NSP
U. S. Atomic Energy Commission
P. O. Box 15132
Cincinnati, Ohio 45215

General Electric Company
U. S. Atomic Energy Commission
310 DeGuigne Drive
Sunnyvale, California 94086

Gulf - General Atomic
U. S. Atomic Energy Commission
P. O. Box 2325
San Diego, California 92112

Oak Ridge National Laboratory
U. S. Atomic Energy Commission
P. O. Box X
Oak Ridge, Tennessee 37830

Pacific Northwest Laboratory
U. S. Atomic Energy Commission
P. O. Box 550
Richland, Washington 99352

Westinghouse Electric Corporation (2)
U. S. Atomic Energy Commission
Advanced Reactors Division
P. O. Box 158
Madison, Pennsylvania 15663

LABORATORIES

Director, LMFBR Program Office (2)
Argonne National Laboratory
9700 South Cass Avenue
Argonne, Illinois 60439

Director, Metallurgy Division (2)
Argonne National Laboratory
9700 South Cass Avenue
Argonne, Illinois 60439

Manager, FFTF Project (2)
Pacific Northwest Laboratory
P. O. Box 999
Richland, Washington 99352

FFTF Fuels Department (2)
Pacific Northwest Laboratory
P. O. Box 999
Richland, Washington 99352

Manager, Chemistry and Metallurgy Division
Pacific Northwest Laboratory
P. O. Box 999
Richland, Washington 99352

Division Leader, Chemistry and Metallurgy Division (CMB)
Los Alamos Scientific Laboratory
P. O. Box 1663
Los Alamos, New Mexico 87544

Director, Metallurgy and Materials Science Division
Brookhaven National Laboratory
Upton, New York 11973

Director, Metals and Ceramics Division (2)
Oak Ridge National Laboratory
P. O. Box X
Oak Ridge, Tennessee 37830

Division Chief, M & S Division
NASA - Lewis Research Center
21000 Brookpark Road
Cleveland, Ohio 44135

Director, Atomics International
Liquid Metal Engineering Center
P. O. Box 309
Canoga Park, California 91304

Division Leader, Inorganic Materials
Chemistry Department
Lawrence Radiation Laboratory
P. O. Box 808
Livermore, California 94551

Manager, Advanced Development Activity
General Electric Company
Knolls Atomic Power Laboratory
P. O. Box 1072
Schenectady, New York 12301

General Manager, Westinghouse Electric Corporation
Bettis Atomic Power Laboratory
P. O. Box 79
West Mifflin, Pennsylvania 15122

CONTRACTORS

Director, LMFBR Technology Program
Atomics International
P. O. Box 309
Canoga Park, California 91304

Associate Manager, Materials Engineering Department
Battelle Memorial Institute
Columbus Laboratories
505 King Avenue
Columbus, Ohio 43201

Director, Nuclear Development Center
The Babcock and Wilcox Company
Atomic Energy Division
Lynchburg, Virginia 24501

Manager, Nuclear Laboratories
Combustion Engineering, Inc.
Nuclear Division
Prospect Hill Road
Windsor, Connecticut 06095

Laboratory Assistant Director
Gulf-General Atomic
P. O. Box 608
San Diego, California 92112

Manager, Plutonium Chemistry and Ceramics Fuels Development
Plutonium Laboratory
Nuclear Materials and Equipment Corporation
Leechburg, Pennsylvania 15656

Manager, Sodium Reactor Technology
General Electric Company
Breeder Reactor Development Operation
210 DeGuigne Drive
Sunnyvale, California 94086

Manager, Research, United Nuclear Corporation
Research and Engineering Center
Grasslands Road
Elmsford, New York 10523

Head, Fuels and Materials
Atomic Power Development Associates
1911 First Street
Detroit, Michigan 48226

K-2 Group Leader
Reactor Division
Los Alamos Scientific Laboratory
P. O. Box 1663
Los Alamos, New Mexico 87544

Irradiations Manager
EBR-II Project
Argonne National Laboratory
P. O. Box 1096
Idaho Falls, Idaho 83401

Director, Vallecitos Nuclear Center
General Electric Company
P. O. Box 846
Pleasanton, California 94566